Erschienen in: Optics Letters ; 43 (2018), 21. - S. 5178-5181
https://dx.doi.org/10.1364/OL.43.005178

High-power frequency comb at 2 μm wavelength emitted by a Tm-doped fiber laser system

C. Gaida,[1,*] T. Heuermann,[1,2] M. Gebhardt,[1,2] E. Shestaev,[1] T. P. Butler,[3] D. Gerz,[4] N. Lilienfein,[3,4] P. Sulzer,[5] M. Fischer,[6] R. Holzwarth,[3,6] A. Leitenstorfer,[5] I. Pupeza,[3] and J. Limpert[1,2,7]

[1]*Institute of Applied Physics, Abbe Center of Photonics, Friedrich-Schiller-Universität Jena, Albert-Einstein-Str. 15, 07745 Jena, Germany*
[2]*Helmholtz-Institute Jena, Fröbelstieg 3, 07743 Jena, Germany*
[3]*Max Planck Institute of Quantum Optics, Hans-Kopfermann-Str. 1, 85748 Garching, Germany*
[4]*Ludwig Maximilians University Munich, Am Coulombwall 1, 85748 Garching, Germany*
[5]*Department of Physics and Center for Applied Photonics, University of Konstanz, D-78457 Konstanz, Germany*
[6]*Menlo Systems GmbH, Am Klopferspitz 19a, 82152 Martinsried, Germany*
[7]*Fraunhofer Institute for Applied Optics and Precision Engineering, Albert-Einstein-Str. 7, 07745 Jena, Germany*
**Corresponding author: christian.gaida@uni-jena.de*

We report on the generation of a high-power frequency comb in the 2 μm wavelength regime featuring high amplitude and phase stability with unprecedented laser parameters, combining 60 W of average power with <30 fs pulse duration. The key components of the system are a mode-locked Er:fiber laser, a coherence-preserving nonlinear broadening stage, and a high-power Tm-doped fiber chirped-pulse amplifier with subsequent nonlinear self-compression of the pulses. Phase locking of the system resulted in a phase noise of less than 320 mrad measured within the 10 Hz–30 MHz band and 30 mrad in the band from 10 Hz to 1 MHz.

Optical frequency combs are of indispensable relevance for precision metrology [1], spectroscopy [2,3], atto-science [4], and related application fields that are constantly explored [5–7]. In parallel, the requirements on optical frequency combs for next generation applications are ever-growing and comprise of wide spectral bandwidth, high power per comb-line, low phase noise and at the same time, high stability, compactness, and environmental robustness. Among the most prominent, robust, and compact sources for optical frequency combs are modelocked Er-doped fiber lasers, which typically cover a spectral region centered at 1.55 μm [8]. Highly nonlinear fibers (HNLF) are often employed for spectral broadening to the whole transparency range of silica fibers (350–2400 nm), but careful attention must be paid to the degradation of spectral coherence and gain of excessive amplitude noise due to the nonlinear processes involved [9,10]. Power scaling of Er-fiber-laser-based frequency combs has so far remained relatively challenging [11] and promising alternatives are found with Yb-doped gain media in the 1 μm wavelength regime providing 10–100 W average power levels [12,13].

Frequency combs at around 2 μm wavelength are currently of tremendous interest for next-generation spectroscopy targeting sensitive detection of certain gases (e.g., CO_2, NH_3) [14,15] and/or to further extend the wavelength coverage of frequency combs to the molecular fingerprint region (3–20 μm) via parametric downconversion in nonlinear crystals [16,17]. With only very few exceptions [18,19], nonlinear crystals with high transmission in the mid-IR (>5 μm) are opaque at around 1 μm wavelength or high-power operation is severely limited by multiphoton absorption, exactly where the most powerful driving lasers operate [20]. It is for that reason that the development of powerful laser sources at wavelengths >1.5 μm are in urgent demand by a large community, which targets next-generation metrology and spectroscopy and relies on powerful frequency combs in the mid-IR. Access to the 2 μm wavelength regime by direct laser emission is possible through thulium- or holmium-doped gain media. Such lasers have recently attained 100 W-class average power in ultrafast operation [21–23], but frequency combs have so far not been realized with average powers beyond the few-W-level [24]. In this work, we present a frequency comb emitted by a Tm-doped fiber chirped-pulse amplification system (TmFCPA) with an unprecedented average output power of 60 W at 100 MHz pulse repetition rate and <30 fs pulse duration, featuring low relative intensity and phase noise.

The experimental setup is schematically depicted in Fig. 1(a) and is comprised of a modelocked Er:fiber oscillator/amplifier (ErFO) (Menlo Systems C-Fiber High Power), a nonlinear broadening stage utilizing a HNLF, a TmFCPA, and a nonlinear solid-core fiber self-compression stage. The seed ErFO provides pulses at 100 MHz repetition rate with a central wavelength of 1.55 μm and allows control over the carrier-envelope-offset frequency (CEO) as well as stabilization of the pulse repetition frequency. An integrated f-2f interferometer is used to lock the ErFO CEO frequency to a flexible master frequency.

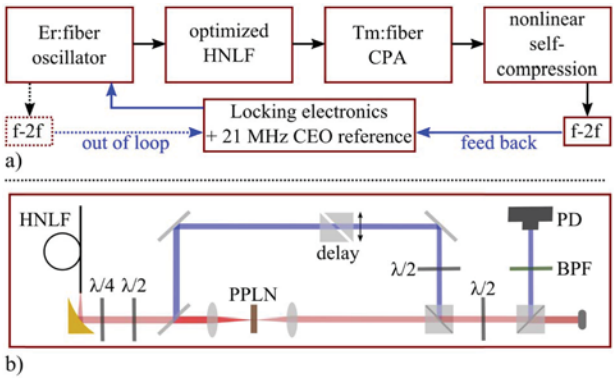

Fig. 1. (a) Schematic of the experimental setup comprising an Er:fiber based modelocked oscillator (ErFO), a highly-nonlinear fiber (HNLF) for coherent spectral broadening to seed the TmFCPA and a nonlinear self-compression stage. A home-built f-2f interferometer provides a beat-note signal, which can be fed back to the ErFO phase locking electronics (feed-back loop). Alternatively, a separate f-2f interferometer can be used to solely phase-lock the ErFO. (b) Setup of the home-built f-2f interferometer. PPLN, periodically poled lithium niobate; BPF, bandpass filter; PD, photodiode.

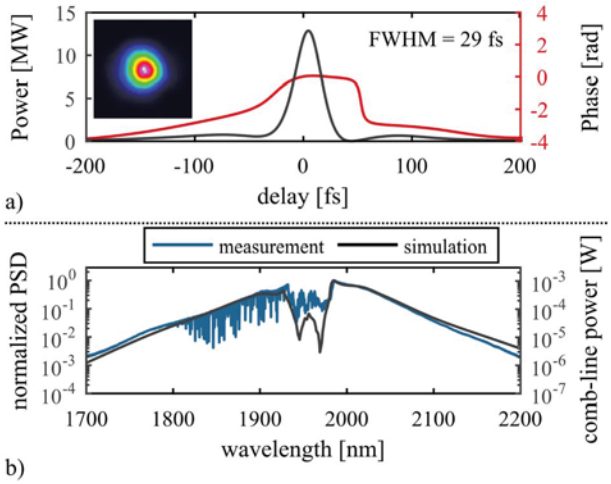

Fig. 2. (a) Simulated pulse and (b) simulated and measured spectra after the nonlinear self-compression fiber output. The measured spectrum shows water absorption features due to transmission through air to the spectrometer. The inset shows the measured beam profile after the nonlinear compression at 60 W of average power.

The output of the ErFO is coupled to a germano-silicate fiber assembly with a core diameter of 4 µm and a length of 7 mm. The short fiber length is beneficial for preserving the coherence of the spectrally broadened output, which extends from 1500 to 2000 nm (–20 dB bandwidth). The pulses are subsequently coupled to an all-fiber pulse stretcher that includes a chirped fiber Bragg grating (CFBG) with a spectral hard-cut of 55 nm (–20 dB bandwidth) centered at 1960 nm. The stretched pulses have a duration of 550 ps (FWHM) and are amplified in a cladding-pumped thulium-doped step index fiber, boosting the average power from 0.05 to 300 mW. The main amplifier is a single-mode, double-clad, Tm-doped photonic crystal fiber with a 3 m length and 36 µm mode-field diameter (MFD). Co-pumping the fiber with 280 W at 793 nm wavelength allows for 90 W of average output power. The amplified pulses are compressed to 250 fs duration in a Treacy compressor with 78% total efficiency (70 W compressed output power). The high-average-power sections of the system are operated in vacuum to avoid detrimental water absorption effects in the atmosphere [25]. The pulse duration is further reduced by incorporating a large pitch fiber [26] with 56 µm MFD and 5.6 cm length as nonlinear self-compression stage.

This self-compression scheme is explained in detail in Ref. [21] and exploits the intrinsic anomalous dispersion of fused silica above 1.3 µm wavelength, which counteracts the positive chirp induced by self-phase modulation. Taking advantage of self-compression of the pulse during its nonlinear broadening requires the optimization of the setup with respect to the pulse peak power, mode-field diameter (MFD), fiber length, and dispersion [21,27]. In order to determine the optimum fiber length of 5.6 cm, we simulated the pulse evolution for a MFD of 56 µm incorporating the laser parameters of the TmFCPA. The simulation is based on solving the non-linear Schrödinger equation including higher-order dispersion, intra-pulse Raman scattering, and self-steepening [28]. Figure 2 shows the simulation result for circular polarization predicting a peak power of 14 MW and a pulse duration of 29 fs, corresponding to 600 nJ pulse energy. The resulting power per comb-line is >1 µW in the spectral range 1700–2200 nm.

The spectrum and frequency-resolved optical gating (FROG) spectrogram of the pulse were measured in air after transmission through a 2 mm potassium bromide (KBr) window with a homemade FROG device. Figure 3 compares the retrieved FROG pulse and spectrum to the simulation, which in this case accounts for the transmission of the pulse through the KBr window. Both the measured spectrum and the FROG retrieval show excellent agreement with the simulated pulse.

The carrier-envelope phase stability of the compressed output is characterized by generating a beat note in a home-built f-2f interferometer optimized for input pulses at around 2 µm wavelength, which is schematically depicted in Fig. 1(b). A 4% fused-silica Fresnel-reflection of the high power output is sent to the f-2f interferometer setup, which includes a fused-silica HNLF with a core diameter of 4 µm, zero dispersion wavelength of 1560 nm and 8 cm length. The power level to the HNLF is further reduced with a pinhole. The HNLF-output contains a dispersive wave centered at 980 nm wavelength, which is separated from the remaining long wavelength output with a dichroic mirror and sent to the first interferometer arm which additionally contains two fused silica wedges for fine tuning of the temporal delay. The long wavelength part of the spectrum is focused into a periodically poled lithium niobate crystal for second harmonic generation (SHG). The dispersive wave and the SHG signal are combined in a polarizing beam splitter and brought to interference in a second polarizing beam splitter. A 10 nm optical bandpass filter centered at 980 nm supresses non-overlapping spectral components of the two beams. An amplified InGaAs photo-diode (Thorlabs PDA05CF2) is used for characterizing the RF spectrum.

In a first step, the ErFO is phase-locked utilizing the beat-note of the integrated f-2f interferometer while the rest of the system is operated "free-running". The home-built f-2f interferometer is optimized to measure a high contrast beatnote after the nonlinear compression stage for <30 fs pulses at 60 W of

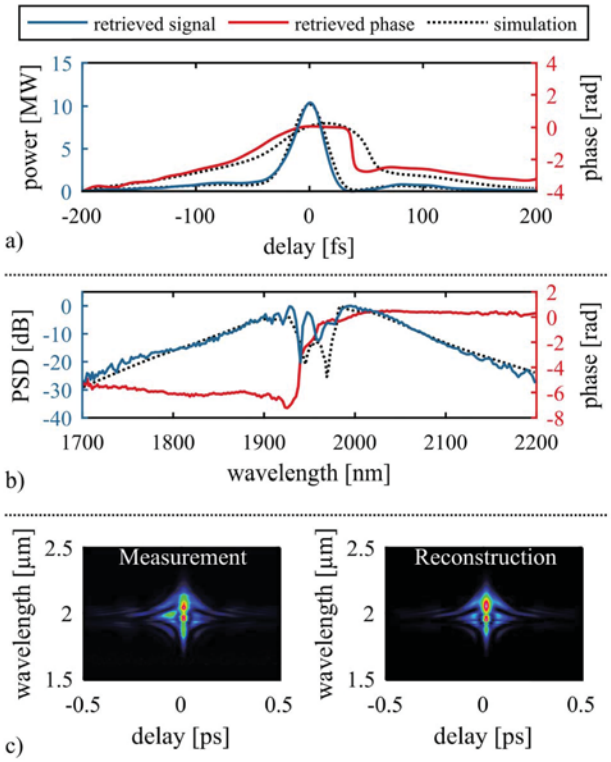

Fig. 3. Retrieved SHG-FROG showing (a) temporal and (b) spectral intensity and phase measured after 2 mm KBr window and comparison to the simulation. (c) Measured and reconstructed FROG-Traces.

average output power. Critical optimization parameters for obtaining the highest possible beatnote contrast are good spatial, temporal and spectral overlap of the interfering pulses. With a resolution bandwidth (RBW) of 300 kHz, a beatnote with 28 dB signal to noise ratio (SNR) is obtained [Fig. 4(a)]. A detailed scan at 50 Hz RBW reveals a SNR of the beatnote exceeding 50 dB [Fig. 4(b)]. The obtained RF signal from the home-built f-2f interferometer is electronically filtered with a low-pass filter in order to obtain the maximum information on the phase stability up to 30 MHz. For "in-loop" phase

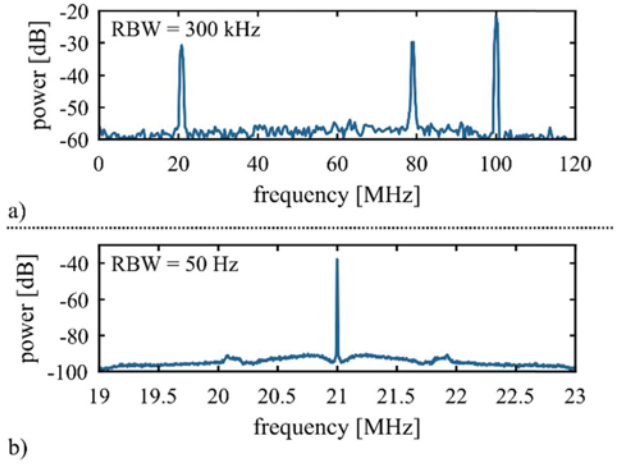

Fig. 4. Measured RF-signals of the f-2f interferometer after the nonlinear compression stage at 60 W of average output power with a resolution bandwidth (RBW) (a) of 300 kHz and (b) of 50 Hz.

stabilization of the entire system to the CEO-frequency of 21 MHz, the ErFO was locked to the signal provided by the f-to-2f interferometer at the CPA output.

The phase stability of the system is analyzed in two steps. At first, the phase stability of the actively phase-locked ErFO is determined. Figure 5(a) shows the power spectral density (PSD) and integrated phase noise of the ErFO, which is obtained from the RF-spectrum of the integrated f-2f interferometer. The phase stability is <100 mrad for an RF-span of 10 Hz–30 MHz and the most noise is accumulated between 100 kHz and 30 MHz with the upper limit due to the low-pass characteristics of our measurement setup. In a second step, the beatnote generated by the home-built f-2f interferometer is sent to the locking electronics for in-loop stabilization of the entire system while the system delivers 30-fs pulses and 60 W of average power. Figure 5(b) (top) visualizes the power spectral density (PSD) and integrated phase noise revealing a phase stability of 320 mrad within a 10 Hz–30 MHz frequency range. Similar to the observation of the phase noise measurement of the ErFO alone, most noise contributions are accumulated at frequencies between 100 kHz and 30 MHz. Several conclusions can be drawn from this observation. Relatively slow phase instabilities at frequencies <100 kHz, that are added by the system components after the ErFO, can be sufficiently corrected by the locking mechanism during in-loop operation. The higher frequency noise >100 kHz is already weakly present at the ErFO and is obviously enhanced in the subsequent parts of the system. In order to investigate the source of the high-frequency noise, we have additionally measured the amplitude noise of the high-power nonlinearly compressed output. The result is depicted in Fig. 5(b) (bottom) revealing a total relative intensity noise (RIN) of less than 0.5%. Amplitude noise contributions are found at low frequencies <100 Hz, which are likely caused by slow beam fluctuations

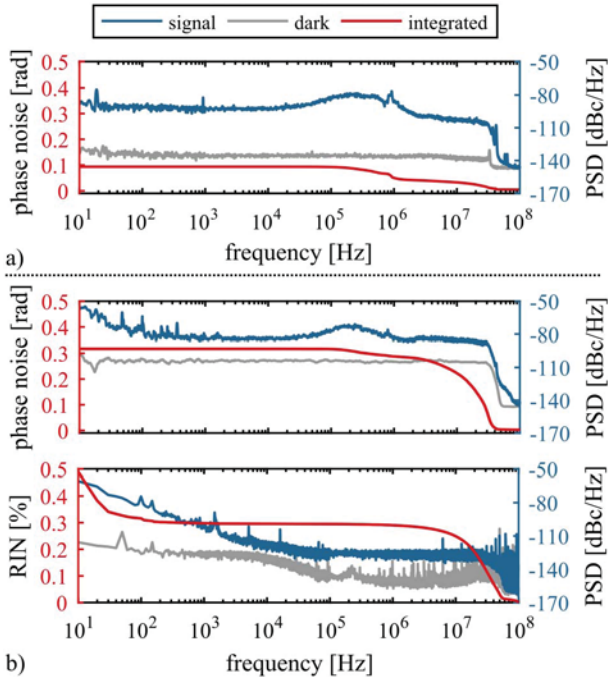

Fig. 5. Measurement of the carrier-envelope phase noise of (a) the oscillator only. (b) The entire system in loop (top) and the amplitude noise spectrum (bottom) at 60 W of average output power.

or vibrations in the TmFCPA. Interestingly, the main noise contribution is detected at frequencies >10 MHz. The presence of high frequency amplitude noise obviously impacts the phase noise measurement in the f-2f interferometer. We have verified this in two different ways. First, we block either arm of the f-2f interferometer and found that the high-frequency noise, although weaker than before, was still detected. Second, we detuned the delay in the f-2f interferometer until the beatnote disappeared completely, which resulted in a remaining broad noise floor. From this it is possible to estimate the total contribution of amplitude noise that contributes to the measured integrated phase noise value of 320 mrad, which is on the order of 20%–30%. It is important to note that the power of the broad noise floor significantly increased when optimizing the delay of the f-2f interferometer for highest beatnote contrast, which clearly indicates that the broad high frequency noise exists both as phase and amplitude fluctuations.

Although it is difficult to conclusively identify the origin of the white-noise-like phase and amplitude instability, several possibilities can be named. Other studies have previously observed that quantum noise in nonlinear processes (e.g., modulation instability) can lead to white-noise-like fluctuations of phase and amplitude [9,10]. Additionally, if amplitude noise is present prior to nonlinear processes, a coupling to phase noise can be expected [9,10,28]. As a consequence, white-noise-like instability contributions are accumulated in the nonlinear broadening stage prior to the TmFCPA or at the high-power nonlinear self-compression after the TmFCPA or even in the HNLF utilized in the f-2f interferometer. In fact, we have observed that reducing the HNLF length in the broadening stage after the ErFO prior to the TmFCPA helped to reduce the white noise contribution, which is equivalent to minimizing the loss of coherence during the nonlinear broadening process. Further improvements could be achieved by optimizing the system prior to this broadening stage with respect to amplitude noise and shortest possible pulse duration. These approaches have been extensively discussed in Refs. [10,29]. Another promising possibility is to avoid nonlinear processes whenever possible, e.g., by utilizing the direct emission of a phase-lockable thulium-doped fiber oscillator [30]. Moreover, we have observed a slight degradation of 2–3 dB of the beatnote contrast at 300 kHz RBW from the f-2f interferometer when operating at the final system output parameters (<30 fs, 60 W) as compared to slightly lower power values/slightly longer pulses. We expect that further improvements of the system stability in terms of amplitude noise can lead to even higher phase stability in the future.

The laser system presented in this Letter provides a frequency comb with broad spectral coverage (1700–2200 nm), ultrashort pulse duration (<30 fs), and high average power (>60 W). In comparison to conventional characterization of phase stability published elsewhere [24], the system provides <30 mrad and <0.2% RIN in an RF-band spanning 10 Hz–1MHz, which is a remarkable result considering the high power per combline of >1 μW. In the course of our study, we have unveiled the necessity to expand the noise characterization to the high frequency realm for fiber-based sources that involve nonlinear processes. We have optimized the system with regard to phase and amplitude noise by following known approaches [9,10,28] and have demonstrated a high phase stability of 320 mrad and low RIN <0.5% in an RF-band spanning 10 Hz–30 MHz. The presented laser is an ideal laser source for metrology and spectroscopy with unprecedented acquisition time and sensitivity in the 2 μm wavelength regime. Furthermore, this source can be utilized for parametric mid-IR generation paving the way for powerful frequency combs in the molecular fingerprint region (2–20 μm).

Funding. Bundesministerium für Bildung und Forschung (BMBF) (13N13973); Deutsche Forschungsgemeinschaft (DFG) (2101); Helmholtz Institute Jena.

Acknowledgment. We thank Prof. Dr. Ferenc Krausz for financial support and fruitful discussions. We thank Nils Geib for help with the FROG retrieval.

REFERENCES

1. T. W. Hänsch, Rev. Mod. Phys. **78**, 1297 (2006).
2. S. A. Diddams, L. Hollberg, and V. Mbele, Nature **445**, 627 (2007).
3. M. J. Thorpe, K. D. Moll, R. J. Jones, B. Safdi, and J. Ye, Science **311**, 1595 (2006).
4. Z. Chang and P. Corkum, J. Opt. Soc. Am. B **27**, B9 (2010).
5. S. A. Diddams, J. Opt. Soc. Am. B **27**, B51 (2010).
6. N. R. Newbury, Nat. Photonics **5**, 186 (2011).
7. S. Keiber, S. Sederberg, A. Schwarz, M. Trubetskov, V. Pervak, F. Krausz, and N. Karpowicz, Nat. Photonics **10**, 159 (2016).
8. F. Tauser, A. Leitenstorfer, and W. Zinth, Opt. Express **11**, 594 (2003).
9. A. Klose, G. Ycas, D. L. Maser, and S. A. Diddams, Opt. Express **22**, 28400 (2014).
10. J. M. Dudley, G. Genty, and S. Coen, Rev. Mod. Phys. **78**, 1135 (2006).
11. H. Timmers, A. Kowligy, A. Lind, F. C. Cruz, N. Nader, M. Silfies, G. Ycas, T. K. Allison, P. G. Schunemann, S. B. Papp, and S. A. Diddams, Optica **5**, 727 (2018).
12. T. Saule, S. Holzberger, O. De Vries, M. Plötner, J. Limpert, A. Tünnermann, and I. Pupeza, Appl. Phys. B **123**, 17 (2016).
13. O. Pronin, M. Seidel, F. Lücking, J. Brons, E. Fedulova, M. Trubetskov, V. Pervak, A. Apolonski, T. Udem, and F. Krausz, Nat. Commun. **6**, 6988 (2015).
14. A. Parriaux, K. Hammani, and G. Millot, Commun. Phys. **1**, 17 (2018).
15. J. T. Hodkinson and P. Ralph, Meas. Sci. Technol. **24**, 1 (2013).
16. A. V. Muraviev, V. O. Smolski, Z. E. Loparo, and K. L. Vodopyanov, Nat. Photonics **12**, 209 (2018).
17. K. F. Lee, C. J. Hensley, P. G. Schunemann, and M. E. Fermann, Opt. Express **25**, 17411 (2017).
18. O. Kara, L. Maidment, T. Gardiner, P. G. Schunemann, and D. T. Reid, Opt. Express **25**, 32713 (2017).
19. I. Pupeza, D. Sánchez, J. Zhang, N. Lilienfein, M. Seidel, N. Karpowicz, T. Paasch-Colberg, I. Znakovskaya, M. Pescher, W. Schweinberger, V. Pervak, E. Fill, O. Pronin, Z. Wei, F. Krausz, A. Apolonski, and J. Biegert, Nat. Photonics **9**, 721 (2015).
20. H. Pires, M. Baudisch, D. Sanchez, M. Hemmer, and J. Biegert, Prog. Quantum Electron. **43**, 1 (2015).
21. C. Gaida, M. Gebhardt, F. Stutzki, C. Jauregui, J. Limpert, and A. Tünnermann, Opt. Lett. **40**, 5160 (2015).
22. J. Zhang, K. Fai Mak, N. Nagl, M. Seidel, D. Bauer, D. Sutter, V. Pervak, F. Krausz, and O. Pronin, Light Sci. Appl. **7**, 17180 (2018).
23. F. Stutzki, C. Gaida, M. Gebhardt, F. Jansen, A. Wienke, U. Zeitner, F. Fuchs, C. Jauregui, D. Wandt, D. Kracht, J. Limpert, and A. Tünnermann, Opt. Lett. **39**, 4671 (2014).
24. F. Adler and S. A. Diddams, Opt. Lett. **37**, 1400 (2012).
25. M. Gebhardt, C. Gaida, F. Stutzki, S. Hädrich, C. Jauregui, J. Limpert, and A. Tünnermann, Opt. Express **23**, 13776 (2015).
26. J. Limpert, F. Stutzki, F. Jansen, H.-J. Otto, T. Eidam, C. Jauregui, and A. Tünnermann, Light Sci. Appl. **1**, e8 (2012).
27. S. V. Chernikov, E. M. Dianov, D. J. Richardson, and D. N. Payne, Opt. Lett. **18**, 476 (1993).
28. J. C. Travers, M. H. Frosz, and J. M. Dudley, *Supercontinuum Generation in Optical Fibers* (Cambridge University, 2010).
29. N. R. Newbury and W. C. Swann, J. Opt. Soc. Am. B **24**, 1756 (2007).
30. C. C. Lee, C. Mohr, J. Bethge, S. Suzuki, M. E. Fermann, I. Hartl, and T. R. Schibli, Opt. Lett. **37**, 3084 (2012).